Testing and quality protocols of 3-folded x-y hodoscope

F. A. Sánchez*, G. Medina-Tanco*, A. D. Supanitsky*, J. C. D'Olivo*, A. Guzman*, G. Paic*, E. Patiño Salazar*, E. Moreno Barbosa†, H. Salazar Ibarguen†, J. F. Valdés-Galicia‡, A. D. Vargas Treviño§, S. Vergara Limón§, L. M. Villaseñor¶

*Inst. de Ciencias Nucleares, Universidad Nacional Autónoma de México, México, D.F., C.P. 04510.
†Fac. de Ciencias Físico Matemáticas, Benemérita Universidad Autónoma de Puebla, Puebla, México.
‡Inst. de Geofísica, Universidad Nacional Autónoma de México, México, D.F., C.P. 04510.
§Fac. de Ciencias de la Electrónica, Benemérita Universidad Autónoma de Puebla, Puebla, México.
¶Inst. de Física y Matemáticas, Universidad Michoacana de San Nicolás Hidalgo Morelia, México.

***Abstract*. Hodoscopes are widely used in cosmic ray experiments. Their main features are tracking and identification of particles. In this work we present detailed testing, building and quality assessment protocols of an hodoscope composed by 294 detection channels distributed over 3 x-y planes. This detector is currently being built in order to study the muon component of cosmic ray showers at ground level. The basic unit of the presented device consists of a MINOS-type scintillator strip with an embedded 1,5 mm diameter Bicron BC92 optical fiber, one pixel of a multianode H7546B Hamamatsu photomultiplier and a fast front-end electronic.**

***Keywords*: Detector testing, Hodoscope, Scintillator**

I. Introduction

Detectors with x-y sensitivity are commonly used in cosmic ray physics. Using solid plastic scintillators in such kind of devices has became an attractive solution in several experiments [1], [2], [3], [4] for many purposes. Among the most outstanding advantages we can quote: (a) simple and robust construction, (b) long term stability, (c) ease of transport and calibration, (d) high efficiency, (e) fast timing features and (e) reliability. Most of the times, spatial resolution is achieved by segmenting the scintillator in strips (normally ranging from 10cm to 4-5m long) having no more than a few centimeter of width and thick (typical cross section areas are $\sim$5-10cm^2). It is of usual practice to assemble a variable number of strips in modules of different shapes and sizes in order to assert the requirements of any specific experimental geometry. Generally, read-out systems are composed by an extra wavelength shifter optical fiber embedded in the strips and coupled to multi-pixel photodetectors (which allows, for example, to place the sensitive part of the detector inside magnetid fields that can corrupt the photodetectors).

In the present work, we report on quality and testing protocols specially conceived to build a small scintillator hodoscope composed by 3 x-y modules of 98 strips. The strips of the detector presented here are 2m long, 4cm wide, 1cm thick and are co-extruded with a thin outer layer of TiO_2 for increasing the reflectivity. Each one has embedded a 1,5 mm diameter Bicron BC92 optical fiber. The read-out is performed by a multianode H7546B Hamamatsu photomultiplier tube plugged to a fast front-end electronic board where a pulse height threshold trigger is applied and the digitilization of the signal occurs.

Although the complexity of the detector proposed, the protocols here described can be faced with reduced man-power and with no need of dedicated machines.

In section II the procedures for cutting, testing and gluig the fibers to the strips are detailed. The photomultiplier and the strip tests are described in sections III and IV respectively. Finally in section V the quality response of the front-end board is presented.

II. Optical Fiber

To build one x-y hodoscope's plane of the type above described are needed at least 280m of optical fiber. (considering also the binding to reach the PMT). The overall detectors fiber requirement is $\approx$850m. Because the manufacturer generally send rolls of $\sim$1km of fiber, we estalished, as a standard procedure to minimize the waste, to cut the fiber in pieces of equal length. We choose 3.5m as the protocol cutting length. In this way, fibers can be cut, tested, polished and, eventually, accepted or discarded before going to the gluing phase.

An efficient cut is made using a razor blade knife, although a lot of care is needed to avoid cladding chiping. The proper way to cut the optical fiber is to pull the fiber tautly and then cut it with the knife perpendicular to the fiber axis. After cleaving, the optical fiber must be inspected using a magnifying glass to assure that the cladding still wraps around the core with no protrusion at the edge of the fiber end.

Among the others fiber's procedures, the polishing is of outmost importance. Before being glued, the fiber tips must be carefully polish in such a way to assure a flat and perpendicular tip with respect to fiber axis. This is a very delicated issue because a slant (or dirty and rough) tip can never be well coupled to the PMT photo-cathode resulting in considerably light loss. To hold the fiber firmly and always prependicular to a glass plane we designed a polishing disc made of stainless. The tip smoothness was achieved using consecutively

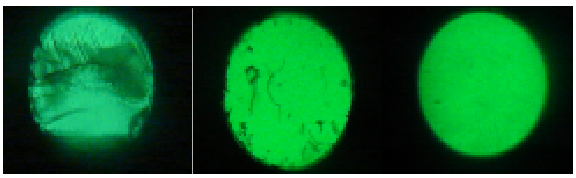

Fig. 1. Polishing steps: (left) rough cut, (middle) polished but dirty and (right) polished and clean fiber.

three different sandpapers: first a 2000-grit film, then a 3μm and finally a 0.3μm film. The polishing proceeds as follow: the first step is to place the 2000-grit sandpaper on a cleaned glass plate and drop on its top a few droplets of water; then, about 10 figure-∞ patterns must be drawn with the fiber (previously introduced into the polishing disc) on the sandpaper; once this first process is finished, it is possible to continue with the finer films following the same procedure as before. In between every step, the fiber and the polishing disc must be cleaned with non-ionized water and a lint-free towel. An example of how are the fiber tips after each polishing step is shown in Fig.1.

We also measured the fiber spectrum using a spectrometer and a blue LED. Fig.2 shows the results. As expected, the fiber shifts the blue light towards the green light (from 475 nm to 510 nm approximately).

The attenuation length of the fibers was measured using a moving LED with a hole specially drilled in order to let the testing fiber move in it. The fiber was fixed by its extremes inside a black box of 4m long and one of the extremes was put in contact with a phototransistor (to improve the coupling we used a drop of optical grease). The attenuation lenght was extracted from a fit to the measured phototransistor voltage as a function of the LED position over the fiber (which, in turns, is proportional to the amount of light transmitted). A double exponential function was used as a fitting curve, $A_{tt}(x) = \left(ae^{-x/\lambda_1} + (1-a)e^{-x/\lambda_2}\right)$ .We obtained a short attenuation length λ_1 ≈60cm and a long one, λ_2 ≈800cm. The amount of light absorbed within λ_1 is a ≈30%.

The light collection in the PMTs strongly depends on the care taken in the manipulation and cleaning of the optical fibers, the grooves, and on the uniformity with which the glue is distributed along the groove. The glue used was EPO-TEK 301-1, a thermosetting epoxide polymer that polymerizes when is mixed with a catalyzing agent or hardener [5]. A clean room was arranged in order to keep the fibers and the strips free of dirt. The drying time is about one day at 23° C.

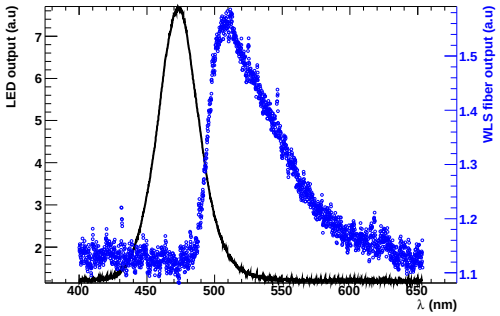

Fig. 2. Blue LED spectrum (solid black line) shifted towards green light by the WLS fiber (open gray circles).

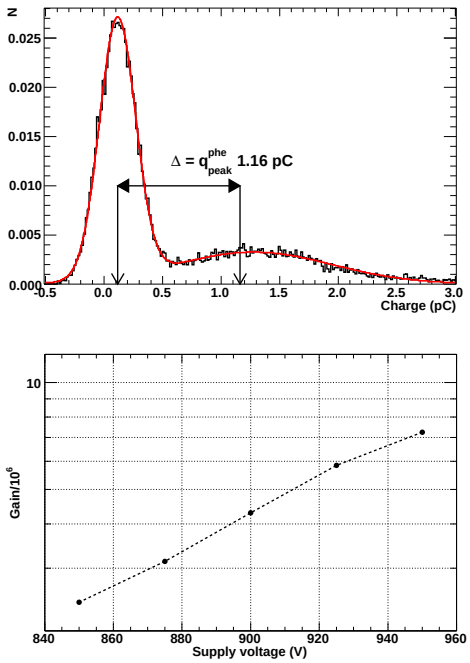

Fig. 3. Single photo-electron spectra for 950V supplied PMT voltage (top) with its fit result superimposed, and PMT gain as a function of supplied voltage (bottom).

III. PMT

We test the Hamamatsu multianode photomultiplier H7546B tube [7]. The main features of this device are: (a) 8×8 multianode with 2mm×2mm anode size, (b) effective area: 18.1mm × 18.1mm, (c) high speed response, (d) low cross-talk (2% typical), and (e) high cathode sensitivity. We start checking the gain of the PMT as a function of supplied voltage. We excited the WLS fiber with a UV LED in order to match the fiber emission spectrum at the level of one single photo-electron. We recorded 50,000 output pulses for each supplied PMT voltage ranging from 825V to 950V. We calculated the pulse charge distribution for each voltage. The case of 950V is shown in the top panel of Fig.3. The Gaussian peak around zero in the figure is the charge distribution of the baseline, while the shoulder peak on its right is the single photo-electron charge distribution. The charge histogram were fit with [6]

$$\sum_{n}^{n_{tot}} \sum_{m}^{m_{tot}} P(n|N_{phe}) \times P(m|n\epsilon) \times N(q - q^{m}_{peak}, \sigma^{m}). \quad (1)$$

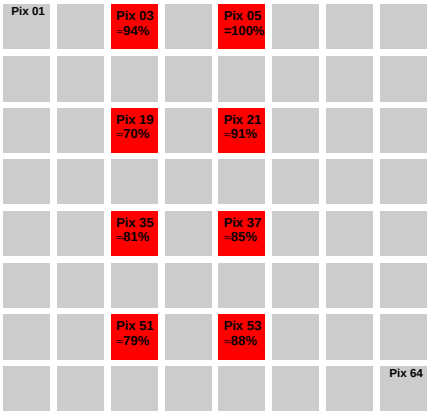

Fig. 4. PMT relative pixel uniformity

$P(n|N_{phe}) = \frac{(N_{phe})^n e^{-N_{phe}}}{n!}$ is the poisson probability of having n photo-electrons pulled out from the photo-cathode if the mean is N_{phe}; similarly $P(m|n\epsilon)$ is the poisson probability of emitting m secondary electrons from the first dynode if the efficiency is ϵ; the contribution of each one of the m electrons after being multiplicated by the consecutive dynodes can be represented as a gaussian $N(q - q^m_{peak}, \sigma^m)$ whose peak position is $q^m_{peak} = m\ eG/\epsilon$ and whose dispersion is $\sigma^m = \sqrt{\frac{m}{\epsilon}} eG/2\epsilon$ (e is the electron charge and G the PMT gain). Using equation (1) combined with a gaussian for fitting the pedestal (and fixing n_{tot}=1 and m_{tot}=1) we found the single photo peak position for each PMT voltage. From the $q^{m=1}_{peak}$ we extracted the gain G. The PMT gain as a function of V is shown in the bottom panel of Fig.3. As expected, G grows exponentially with supplied voltage.

The typical anode response variations, specified by the manufacturer over the whole PMT pixel grid, range from 5% to 30% approximately, being the pixels on the edge the most sensitive. We have check the anode uniformity over 8 significant pixels, i.e., pixels conforming two columns going from the edge towards the center of the pixel matrix. Our results are shown in Fig.4. It can be seen that, in completely agreement with factory specifications, the pixels on the edge are the most sensitive and non-uniformities can reach $\approx$ 30% in the center of the grid.

As previously mentioned, the cross talk between neighboring pixels quoted by the manufacturer is smaller than 2%. Nevertheless, since our optical fiber has a diameter of 1.5mm the cross-talk could be an issue. Cross talk features have several implications on detector efficiency and therefore must be very well known and characterized. Trigger as well as physics analisys of the hodoscope we are presenting depend on a good undertanding of cross talk. To find the cross talk, we injected light in a single pixel and we recorded the output from that stimulated pixel and from two of its neighbours (we selected those pixels which have the greater cross talk, i.e., the adjacent ones and not the diagonal ones).

TABLE I
EFFICIENCY (PIXEL 1) AND CROSS TALK (PIXELS 2 AND 9) FOR TWO DIFFERET DISCRIMINATION THRESHOLDS.

Pixel	Prob(h $\geq$ h_{thr})	
	h_{thr} = 15 mV	h_{thr} = 20 mV
1	$\approx$ 94%	$\approx$ 83%
2	$\ll$ 1%	$\ll$ 1%
9	$\approx$ 5%	$\leq$ 2%

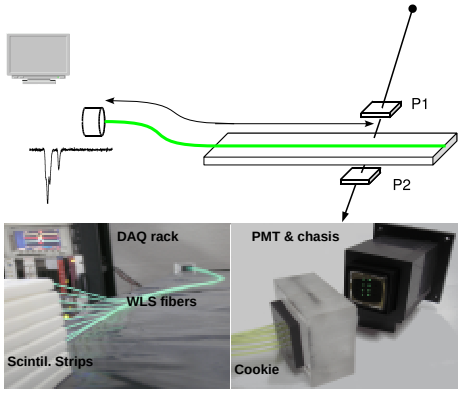

Fig. 5. Top: experimental setup to record real muon signal at a given X distance from the PMT. A coincidence between detectors P1 and P2 triggers the data acquisition. Bottom: strips, fibers and DAQ rack used in the test.

The results are summarized in the table III for 15 mV and 20 mV discrimination thresholds.

IV. STRIP

The easiest way to test one single assembled hodoscope channel, i.e. to test the scintillator strips coupled to a PMT via the WLS optical fibers, is using background muons. The top panel of Fig.5 shows schematically the experimental setup we used. The 16 hole mask (or *cookie*) to couple the fibers to the PMT and the chasis to hold the PMTs inside a dark box are shown in the bottom panel of the same figure. These tools where specially designed for this test and allow a good and stable aligment of the fiber with the PMT anode grid.

A coincidence signal in detectors P1 and P2 (located X centimeters away from the PMT), triggers the readout system: on one hand, complete waveform pulses were stored in the PC through an Tektronix TDS3014B oscilloscope [8] usign a NI-GPIB interface [9]; on the other hand, signals were sent to a CAMAC CMC080 [12] module to measure their charges. The interface towards the PC was a CC32 Wiener crate controller [10]. The acquisition software operates under Ubuntu-6.01 Linux distribution [11].

Because the hodoscope will readout signals from one edge of the scintillator strips, we have to characterize the typical non-unifromity along the longest side of the strips. This *longitudinal* response depends mainly on 2 variables: (a) the reflection that can be achieved at the edges of the strip (where there is no $Ti0_2$ coating) and (b) the extra fiber length needed to join the strip's end with the PMT (which is linked to strip's position in

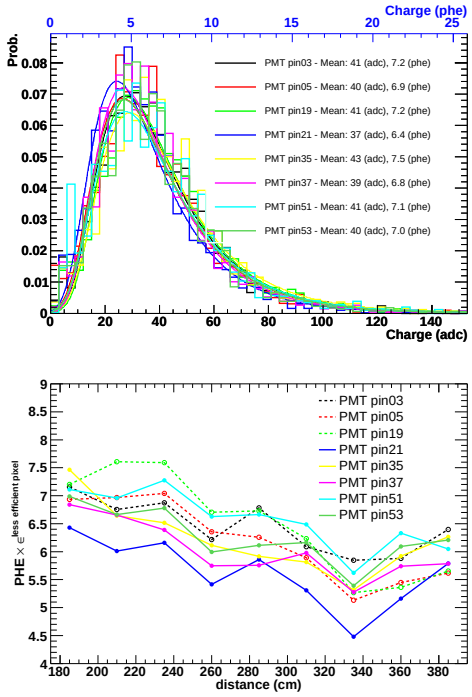

Fig. 6. Charge distribution spectra at 185cm from the PMT (top) and peak positions as a function of the distance (bottom) for 8 different strips.

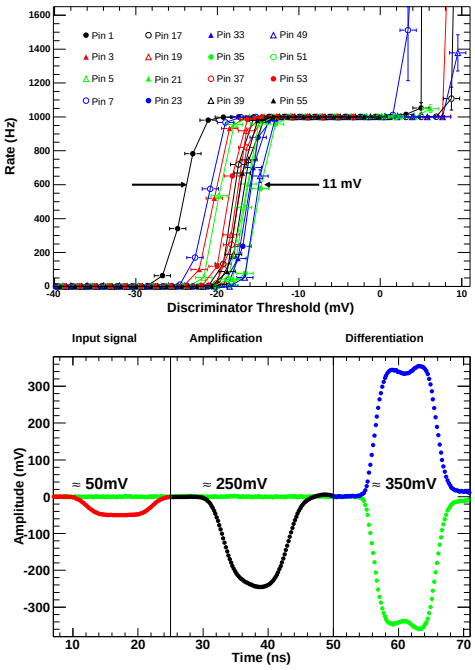

Fig. 7. Testing and characterization measurement on FE board with controlled square pulses of 50 mV height and ≈10 ns width injected at a frequency of 1 kHz.

the x-y plane). We scan the longitudinal response of 8 strips using the setup shown in Fig.5 and varying the distance X from 185cm to 380cm in 25cm step. The distribution spectra at closest distance is shown in the top panel of Fig.6 were the relative calibration between pixels was not taken into account. The behavior of the distribution's peaks as a function of the distance is shown in the bottom panel of Fig.6. To take into account the worst possible scenario, the normalization was done with respect to the less efficient pixel (i.e., pixel 19) which is ≈30% below the best one. It is worth to note that, even in this scenario, we expect that the scintillation light produced at the far end of the strip pulls out, in average, more than 5 photo-electrons from the PMT's cathode.

V. Front End Board

Each stage of the FE board has been tested with controlled square pulses of 50mV height and ∼10ns width. The input pulses were injected at frequency of 1kHz. Averaged output signals were recorded at the amplification and at the differentiation stages. On the other hand, the output rates of all the 64 channels were studied as a function of the discriminator threshold voltage. As an example, the rates of 16 different channels are shown in the top panel of Fig.7. The mean outputs of each electronic stage can be seen in the bottom panel of the same figure.

VI. Conclusions

We have presented several testing protocols to assest the quality requirements of an 3-folded hodoscope based on the scintillation technique. The detector under study have 294 scintillator strips distributed over 3 x-y planes and embedded with WLS optical fibers. Signals are collected by a multipixel photodetector H7546B and digitized by a fast front-end electronic board. The testing procedures are of outmost importance because will allow to optimize the detector response. For example, despite intrinsic strip-to-strip variations a more uniform response can be achieved assinging the scintillator bars with the larger light yield to the PMT's pixels with less efficiency. In this way, the efficiency of the device would be noticeable improved.

Acknowledgements

This work is supported by CONACyT (Mexico). Authors also acknowledge financial aid from UNAM through CIC and DGAPA-PAPIIT grants.

References

[1] D. G. Michael *et al.* [MINOS Collaboration], Nucl. Instrum. Meth. A **596** (2008) 190 [arXiv:0805.3170 [physics.ins-det]].
[2] F. Carminati *et al.*, J. Phys. G **30** (2004) 1517.
[3] B. Cheynis *et al.*, Nucl. Instrum. Meth. A **569** (2006) 732.
[4] C. P. Achenbach and J. H. Cobb, Nucl. Instrum. Meth. A **539** (2005) 112 [arXiv:nucl-ex/0403053].
[5] EPOXY TECHNOLOGY, INC, http://www.epotek.com.
[6] N. Tagg *et al.*, Nucl. Instrum. Meth. A **539** (2005) 668.
[7] Photonics HAMAMATSU, http://www.hamamatsu.com.
[8] Tektronix Inc., http://www.textronix.com.
[9] National Instrument Corporation, http://www.natinst.com.
[10] ARW Elektronik WIeNeR, http://www.wiener-d.com.
[11] ARW Elektronik and Klaus Hitschler, http://he3.dartmouth.edu/pcicc32.
[12] Cheesecote Mountain CAMAC, http://www.cmcamac.com.